Nanoscale Advances

ROYAL SOCIETY OF CHEMISTRY

PAPER

View Article Online
View Journal | View Issue

Cite this: *Nanoscale Adv.*, 2026, **8**, 1423

Tailoring the structural and morphological properties of $LiNi_{0.5}Co_{0.2}Mn_{0.3}O_2$ cathode materials *via* a novel mixed-solvothermal method

Md. Sohel Rana, [a] Abdur Rahim, [a] Rakibul Hasan,[a] M. Shahinuzzaman, [a] Aninda Nafis Ahmed,[b] Md. Saiful Quddus, [c] Chanchal Kumar Roy, [d] Mosharof Hossain [a] and Mohammad Shah Jamal *[a]

$LiNi_{0.5}Co_{0.2}Mn_{0.3}O_2$ (NCM523) is a promising cathode material for lithium-ion batteries with high capacity, stability, and environmental benefits, but conventional synthesis methods often cause structural degradation and cation mixing that hinder performance. In this study, a novel, optimized, and facile mixed-solvothermal approach mediated by ethylene glycol, water, and ethanolamine was employed to synthesize NCM523 cathode materials with enhanced crystallinity and optimized morphology. The effects of different calcination temperatures (700 °C, 800 °C, and 900 °C) on the structural, morphological, and chemical properties were systematically investigated. X-ray diffraction (XRD) analysis confirmed the formation of a well-ordered layered structure, with the sample mediated in ethylene glycol, water and ethanolamine and calcined at 800 °C (NCM-800) exhibiting superior phase purity and minimal cation disorder. The sample calcined at 800 °C exhibited the highest crystallite size of 37 nm and an intensity ratio of 1.42 in the case of the (003) to (104) planes, which indicates the lowest cation mixing of Li^+/Ni^{2+} ions. X-ray photoelectron spectroscopy (XPS) further revealed optimal Ni^{2+}/Ni^{3+} ratios (0.23) and lattice oxygen retention in NCM-800, indicating robust redox activity and minimal oxygen vacancies. Field emission scanning electron microscopy (FE-SEM) demonstrated that NCM-800 possessed uniform, densely packed spherical particles with minimal surface defects, contributing to improved mechanical integrity and electrochemical stability. Compared to samples calcined at lower or higher temperatures, NCM-800 achieved an optimal balance between crystallinity, particle morphology, and structural robustness. These findings highlight the potential of the mixed-solvothermal method as a promising, scalable, and cost-effective strategy for the synthesis of high-performance NCM523 cathode materials, paving the way for their application in next-generation lithium-ion batteries and advanced energy storage systems.

Received 9th October 2025
Accepted 27th December 2025

DOI: 10.1039/d5na00957j

rsc.li/nanoscale-advances

Introduction

The growing demand for electric cars, hybrid electric vehicles (HEVs), portable electronics, and the substantial conversion from fossil fuels to renewable energy sources such as solar, hydropower, geothermal, biofuels, and wind power are central to addressing global climate change and reducing greenhouse gas emissions.[1,2] However, one of the critical challenges related to the intermittent nature of renewable energy generation is that it causes energy production to be inconsistent due to fluctuating weather patterns. This highlights the importance of developing efficient energy storage systems that can store excess energy during peak production and release it when consumption is high or generation is low, thereby driving the demand for advanced energy storage technologies. Lithium-ion batteries (LIBs) are now the most promising options among the many energy sources because of their high specific capacity, large energy density, extended cycle life, affordability, environmental compatibility, relatively lightweight design, and scalability from small devices to large industrial applications.[3–5] Powering everything from laptops and smartphones to electric vehicles and grid-based power storage devices, LIBs are now the cornerstone of contemporary energy storage systems. The performance of these batteries must be improved immediately due to the growing interest in sustainable and clean power

[a]*Institute of Energy Research and Development (IERD), Bangladesh Council of Scientific and Industrial Research (BCSIR), Dr Qudrat-E-Khuda Road, Dhanmondi, Dhaka-1205, Bangladesh. E-mail: msjamal@bcsir.gov.bd*

[b]*Pilot Plant and Process Development Centre (PP&PDC), Bangladesh Council of Scientific and Industrial Research (BCSIR), Dr Qudrat-E-Khuda Road, Dhanmondi, Dhaka-1205, Bangladesh*

[c]*Institute of Glass and Ceramic Research and Testing (IGCRT), Bangladesh Council of Scientific and Industrial Research (BCSIR), Dr Qudrat-E-Khuda Road, Dhanmondi, Dhaka 1205, Bangladesh*

[d]*Department of Chemistry, Bangladesh University of Engineering and Technology, Dhaka-1000, Bangladesh*

sources, especially in the areas of energy density, high performance, safety, and affordability. However, there are still several obstacles to their widespread applications, which call for continued research and development to enhance the basic characteristics of LIBs, particularly in terms of their cathode materials, which are the main active materials of LIBs.

In the past decades, significant progress has been made in the development of cathode materials, with many promising candidates emerging, such as lithium cobalt oxide and phosphate ($LiCoO_2$ and $LiCoPO_4$),[6,7] lithium nickel oxide and phosphate ($LiNiO_2$ and $LiNiPO_4$),[8,9] lithium manganese oxide and phosphate ($LiMnO_2$ and $LiMnPO_4$),[10,11] and lithium iron phosphate ($LiFePO_4$).[12] These materials have been used extensively in commercial batteries because of their stable cycling behavior, high discharge plateau, and moderate energy density and thermal stability. However, their high cost, unavailability for use in high energy density applications, limited supply of cobalt, and mining-related environmental issues have led researchers to seek more affordable and environmentally friendly alternatives. $LiNi_{1-x-y}Co_xMn_yO_2$ (NCM) composites, which have a complex hexagonal $R\bar{3}m$ and monoclinic $C2/m$ structure, have recently drawn a lot of attention due to their higher reversible capacity (>200 mAh g^{-1}), high operating voltage, lower cost, and environmental friendliness by lowering their dependency on cobalt.[13] Among them, $LiNi_{0.5}Co_{0.2}Mn_{0.3}O_2$ (NCM523) has emerged as one of the most promising cathode materials for LIBs because of its notable tolerance to overcharge and discharge, good cycling behavior, reasonable thermal and structural stability, high-rate capability, and relatively high capacity with a dominant plateau at about 4.7 V.[14] Despite these fascinating advantages, the NCM523 cathode material invariably exhibits irreversible structural rearrangement, undesired phase transitions, and structural degradation during charge/discharge cycles, leading to lattice distortion, cation mixing between Li^+ and Ni^{2+} ions, volume change, formation of oxygen vacancies, micro-cracks, and loss of lithium ions, all of which have a substantial impact on the electrochemical performance and, consequently, the commercialization of electrochemical energy storage on a massive scale.[15] It is widely acknowledged that the construction, interfacial stability and cathode material electrochemical effectiveness are significantly influenced by the precursors and conditions of preparation. Based on the aforementioned query, the main strategies to minimize these drawbacks by improving structure and interfacial stability, experimental endeavors such as surface modification,[16] heteroatom substitution by ion doping,[17] morphology design,[8] coating modification,[7] and microwave-assisted synthesis[18] are widely used. Several synthesis methods, including the sol–gel method, solution combustion method,[19] solid-state reaction,[9] spray drying,[10] hydrothermal method,[7] co-precipitation method,[16] and solvothermal method, have been used to ensure optimized morphology, which enhances the electrochemical efficiency of the NCM523 cathode materials. The hydrothermal/solvothermal method is the most promising strategy for researchers to develop nano- and sub-micron cathode materials since it offers comparatively simple and trustworthy reaction conditions by using simple equipment. The ability to achieve high-purity, uniform, and well-structured NCM523 cathode materials with improved control over particle size, shape, and stoichiometry motivates the use of the mixed solvothermal process.[20] It offers an assortment of benefits over alternative synthesis techniques, particularly in terms of electrochemical performance, scalability, and cost-effectiveness, making it a desirable option for advanced battery materials. The structural and electrochemical performance of layered NCM523 cathode materials is strongly influenced by synthesis conditions, particularly the choice of solvent in the solvothermal method. Solvents not only act as dispersing media but also control precursor chemistry, nucleation kinetics, and subsequent crystallization behavior.[21] Metal salt dissolution and complexation, as well as the crystallization process, are greatly influenced by the mixture of water and organic solvents like ethylene glycol (EG), polyethylene glycol (PEG), glycerol, ethanolamine (EA), triethylamine, and ethanol. Among the commonly employed solvents, EG has been widely used due to its high boiling point, viscosity, and ability to act as a polyol reducing agent. In NCM523 and related layered oxides, EG assisted synthesis has been reported to promote uniform precursor formation, enhance the lattice parameter ratio, and reduce cation disorder, thereby improving structural stability and electrochemical capacity.[22] However, the limited hydrolysis ability of EG often leads to incomplete decomposition of metal salts, uncontrolled nucleation, and smaller crystallite sizes, which may result in structural defects and inferior electrochemical performance. To overcome these shortcomings, mixed solvent systems have been explored. The incorporation of water into EG accelerates the hydrolysis of metal precursors, increases ionic mobility, improves reaction homogeneity, and promotes higher crystallinity compared with using EG alone.[23] Beyond binary solvents, the addition of organic amines, particularly EA, has shown further promise in controlling precursor chemistry. Conventional two-component mixtures like EG/H_2O cannot match the synergistic chemical environment provided by the three-component EG/H_2O/EA system. Unbalanced metal-ion precipitation and wide particle-size distributions result from weak coordination, even though EG/H_2O systems offer moderate hydrolysis control. The current system simultaneously balances hydrolysis kinetics, chelation strength, and sol–gel network formation by combining EG, water, and EA. This results in uniform nucleation and synchronized co-precipitation of Ni, Co, and Mn ions, which is not possible in binary systems. EG stabilizes polymeric chains, enhances dispersion, and stops particle overgrowth, water guarantees full but moderated hydrolysis, and ethanolamine offers regulated metal–ligand coordination and pH buffering. In the end, NCM523 cathode materials with improved phase purity, cation homogeneity, and electrochemical performance are produced by a precisely adjusted medium that encourages homogeneous precursor synthesis, narrow particle-size distributions, and cleaner thermal decomposition. It also acts as a pH-controlling agent, thereby regulating hydrolysis and condensation processes during agglomeration, and slows down nucleation and facilitates controlled crystal growth, which reduces cation mixing and enhances layered ordering and crystallinity.[24] The

specific ratio of solvents affects the final morphology, determining whether the particles will form as spheres, rods, or plates, with organic solvents typically encouraging smoother particle growth and more controlled morphology. Additionally, the material's phase formation and crystallinity are affected by the solvent selection; well-optimized solvent systems improve phase purity and suppress the production of undesirable byproducts. The NCM523 cathode materials have been significantly affected by calcination temperature, which determines phase formation, crystallinity, and shape.[25,26] The excessive heat can cause agglomeration and phase transitions, which jeopardize the stability and transport of lithium ions, while the ideal temperatures maximize electrochemical performance.

The development of high-performance NCM523 cathodes that provide elevated battery efficiency relies on this fine-tuning. It is hypothesized that the introduction of EA and EG for the preparation of NCM523 cathode materials would provide a clean, affordable, environmentally friendly, thermally stable, and high-purity material with improved crystallinity and electrochemical performance. Yet, to the best of our knowledge, the combined use of EG, water, and EA as a mixed solvent system for the synthesis of NCM523 has not been reported. To satisfy the above hypothesis, in this investigation, an alternative facile EG, water, and EA mediated mixed solvothermal method has been used to create NCM523 cathode materials and examine how various calcination temperatures affect the end products.

Materials and methods

Materials

All the chemicals were used as supplied, and no additional purification was carried out. Nickel acetate tetrahydrate ($Ni(CH_3COO)_2 \cdot 4H_2O$, 99%), cobalt acetate tetrahydrate ($Co(CH_3COO)_2 \cdot 4H_2O$, 98%), manganese acetate tetrahydrate ($Mn(CH_3COO)_2 \cdot 4H_2O$, 99%), urea ($NH_2$–CO–$NH_2$, 99%), lithium carbonate (Li_2CO_3, 99%), and absolute ethanol were purchased from Sigma-Aldrich, Germany. Ethylene glycol (99.0%) and ethanolamine ($HOCH_2CH_2NH_2$, 99%) were collected from Qualikems, India, and Giant Chem Solution, USA, respectively. Deionized (DI) reverse osmosis and ultraviolet light were used to get water from Pureit (Taiwan).

Experimental

Stoichiometric ratios of $Ni(CH_3COO)_2 \cdot 4H_2O$, $Co(CH_3COO)_2 \cdot 4H_2O$, and $Mn(CH_3COO)_2 \cdot 4H_2O$ (molar ratio was 5 : 2 : 3) were dissolved in a mixture of ethylene glycol, deionized water, and ethanolamine of 80 mL (the volume ratio was 0.5 : 0.25 : 0.25). The initial pH of the solution was 10.5 ± 0.2, which ensured steady hydrolysis. Under vigorous magnetic stirring, a specific quantity of urea (4.5 mmol) was added to the mixture as the chelating and slow-release precipitating agent until all the precursor salts dissolved completely. For comparison, identical stoichiometric ratios of metal acetate salts were separately dissolved in an EG/deionized water mixture (volume ratio: 0.5 : 0.5) and pure EG solvent (80 mL). After that, the mixture was placed in a 100 mL Teflon-lined stainless-steel autoclave (the filling capacity was fixed at around 80%), placed in a heating oven and heated to 160 °C for 20 hours in order to produce the carbonate precursor. After the mixed solvothermal reaction, the precipitated product was cooled naturally to room temperature, centrifuged at 5000 rpm, washed three times with deionized water and ethanol each, and dried at 55 °C in a vacuum oven for 24 h. The as-obtained carbonate precursor was powdered, and an appropriate amount of Li_2CO_3 was mixed (lithium carbonate to precursor molar ratio = 1.05 : 1) thoroughly in an agate mortar, and the obtained final precursor was annealed at 450 °C for 5 h in a muffle furnace. Once the precursor mixture had naturally cooled to ambient temperature, it was equally ground once again and finally calcined at a certain temperature (700 °C, 800 °C, and 900 °C) for 12 h in the presence of air with a ramp rate of 20 °C min^{-1}. The NCM523 cathode materials were allowed to cool to room temperature and ground with 5 mm stainless steel balls in a 10 : 1 ball-to-powder ratio in a planetary ball mill (Pulverisette 23, FRITSCH, Germany) at 50 Hz for 5 min with 15 balls (total 3.15 g). The typical solid-state product yield was 37–40.5%, depending on the solvent system and calcination temperature. The resulting powder was then collected and stored in an airtight container for characterization and fabrication of the electrode. The cathode materials were denoted as NCM7, NCM8, and NCM9 according to the calcination temperatures of 700 °C, 800 °C, and 900 °C, respectively.

Materials characterization

The surface structure and particle size distributions of the prepared NCM523 cathode ingredients were analyzed by using a field-emission scanning electron microscope (FE-SEM, JEOL-7610F, Japan), operated at 15 kV, followed by ImageJ-based statistical analysis of 100–150 particles to ensure accurate morphology and size quantification. EDX spectra were taken with an energy-dispersive X-ray spectroscopy adaptor coupled to a FE-SEM instrument (JEOL-JED2300 Analysis Station, Japan) operated at 15 kV. The surface elemental composition was investigated by X-ray photoelectron spectroscopy (XPS, K-alpha, Thermo Scientific™, USA). X-ray diffraction (XRD, Panalytical, EMP3, Netherlands) patterns of the powder samples were used to determine the crystalline size and sample constituents.

Results and discussion

The impact of organic solvent composition on the crystallite size and phase purity of the synthesized NCM523 cathode materials is clearly demonstrated by the XRD results, as shown in Fig. 1. The diffraction patterns of all three cathode materials in three different solvent mixtures show peaks at two theta values of 18.93, 36.60, 37.57, 38.02, 44.40, 48.65, 59.70, 64.38, 64.78, and 68.19 corresponding to the lattice planes of 003, 101, 006, 102, 104, 105, 107, 108, 110, and 113, respectively. All of these patterns accurately resemble the combined identical phases of the cubic structure with the space group $Fd\bar{3}m$ of $Li_2CoMn_3O_8$ (JCPDS no. 48-0261), the rhombohedral structure (hexagonal axes) with the space group $R\bar{3}m$ of $LiNiO_2$ (JCPDS no.

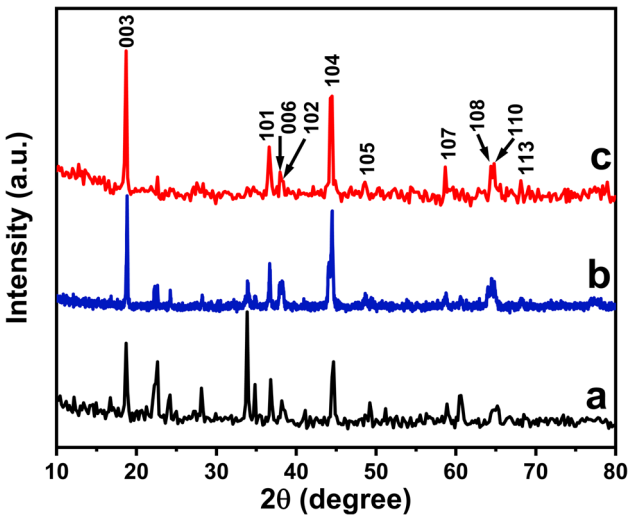

Fig. 1 XRD diffraction patterns of NCM523 cathode materials synthesized using three solvent environments of (a) EG, (b) EG and water, and (c) EG, water, and EA.

09-0063), and the monoclinic crystal system with the space group $C2/c$ of $Li_{1.33}Mn_{0.67}O_2$ (JCPDS no. 27-1252).[23] When EG alone was used as the reaction medium, the diffraction pattern (Fig. 1a) displayed relatively broad and less intense peaks, together with several minor secondary reflections. Such features are typically associated with smaller crystallite size, incomplete crystallization, and the presence of undesirable impurity phases such as spinel or rock salt-type oxides. The poor crystallinity can be attributed to the fact that, while serving as both solvent and a mild reducing agent, it provides limited hydrolysis capability and insufficient control over metal ion distribution. Consequently, the nucleation process occurs rapidly and homogeneously, leading to increased cation mixing, structural disorder, and suppressed long-range ordering in the layered lattice. The addition of water to EG produced a notable improvement in crystallinity and phase purity (Fig. 1b). The XRD peaks became sharper and more intense, while the background noise and impurity reflections were significantly reduced. This enhancement can be rationalized by the role of water in promoting hydrolysis and increasing ionic mobility, which results in more uniform mixing of Ni, Co, and Mn ions within the precursor solution.[23] A more homogeneous precursor composition facilitates a more controlled nucleation process during subsequent heat treatment, thereby yielding larger crystallites with reduced defect concentrations. This observation highlights the synergistic role of water in complementing EG by enhancing the solvation and reactivity of the metal ions. The best structural characteristics, however, were achieved when EA was introduced into the EG–water solvent system (Fig. 1c). The XRD pattern of this sample showed the sharpest reflections with well-resolved splitting of the (006)/(102) and (018)/(110) doublets, which is the most reliable indicator of the formation of a highly ordered layered $Fd\bar{3}m$ structure.[27] EA provides multiple benefits by strongly chelating transition metal ions to prevent premature precipitation, simultaneously acting as a pH buffer to stabilize the reaction medium and moderate hydrolysis rates, while also retarding nucleation kinetics to facilitate uniform and controlled crystal growth. These effects collectively suppress cation disorder, particularly the migration of Ni^{2+} into Li^+ sites, and eliminate residual impurity phases. The superior ordering obtained in the EG, water, and EA system suggests reduced Li^+/Ni^{2+} cation mixing, which is crucial for ensuring high lithium-ion mobility and electrochemical performance. The degree of cation ordering in the prepared NCM523 samples was assessed *via* the intensity ratio of the (003) and (104) diffraction peaks, which serves as a consistent indicator of Ni^{2+}/Li^+ cation mixing. The NCM523 synthesized using the EG-only solvent system displayed an intensity ratio of 1.23, signifying a moderately ordered layered structure. The two-solvent system (EG + H_2O) exhibited a little lower ratio of 1.10, representing comparatively higher cation mixing and abridged structural ordering. In contrast, the three-solvent system (EG + H_2O + EA) generated a significantly higher ratio of 1.42, which surpasses the commonly acknowledged threshold (1.2) for well-ordered $R\bar{3}m$ type layered oxides. Therefore, the three-solvent combination route demonstrates superior structural optimization and is the most appropriate solvent atmosphere for reaching high-quality NCM523 cathode materials.

FTIR investigation reveals that the solvent environment strongly impacts the removal of residual functional groups and the formation of the metal–oxygen lattice (Fig. 2). The precursor of NCM523 cathode materials, synthesized only in EG, shows strong O–H stretching (at around 3400 cm^{-1}) and bending (at around 1620 cm^{-1}) bands. This precursor also gives a robust C–O stretching band at 1130 cm^{-1} and bending vibrational mode at 865 cm^{-1}, along with a weak metal oxygen (M–O) vibrational mode arising from Ni, Co, and Mn within the layered oxide lattice in the region of 520–650 cm^{-1}, indicating unfinished decomposition.[28] Adding water to EG significantly decreases hydroxyl intensity and improves M–O vibrations due

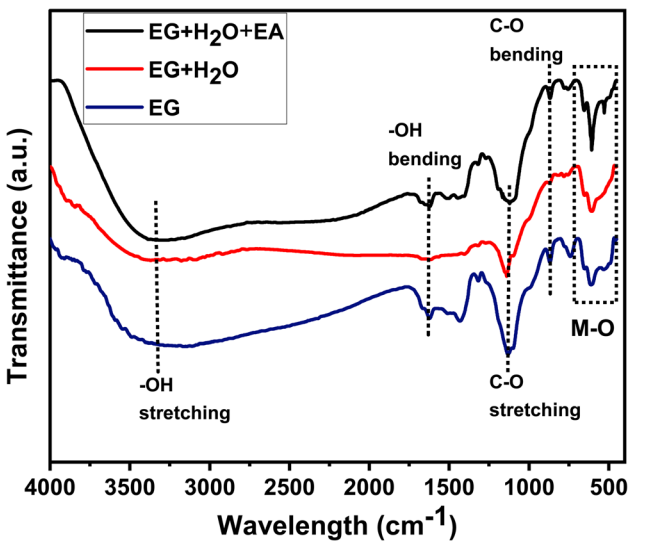

Fig. 2 FTIR spectra of NCM523 cathode materials synthesized using three solvent environments.

Table 1 Effect of the solvent environment on NCM523 cathode materials

Sample conditions	O–H vibrations (3400 and 1620 cm^{-1})	C–O vibrations (1130 and 865 cm^{-1})	M–O bands (520–650 cm^{-1})	Interpretation
EG	Strong	Strong	Weak	Poor precursor decomposition, disordered network
EG + H_2O	Moderate	Reduced	Improved	Better hydrolysis and coordination
EG + H_2O + EA	Lowest	Strongly suppressed	Strongest and sharpest	Highly uniform precursor, best structural development

to enhanced metal-ion hydrolysis. However, the three solvent system (EG + H_2O + EA) offers the cleanest FTIR profile, showing strongly suppressed O–H and C–O vibrations and the sharpest M–O vibrational bands, confirming superior precursor homogeneity and more efficient metal–ligand coordination (Table 1). Therefore, the three solvent-derived (EG + H_2O + EA) precursor was selected as the most reliable synthesis pathway, and all subsequent stages of this study, including calcination at three different temperatures and comprehensive structural and morphological characterization, were carried out using this optimized material.

The thermal decomposition behavior of the NCM523 carbonate precursor was estimated by TGA, and the resulting curve displays three distinct mass-loss regions characteristic of solvothermally derived mixed-metal carbonates (Fig. 3). The first minor weight loss below 200 °C resembles the evaporation of physically adsorbed moisture and residual solvent molecules from the precursor surface. A more noticeable mass loss is observed between 200 and 450 °C, which is attributed to the decomposition of organic species originating from the solvothermal medium and the partial breakdown of metal-carbonate intermediates. A major decomposition step occurs between 500 and 750 °C, connected with the complete decarboxylation of lithium carbonate and the formation of Co, Ni, Mn, and Li oxide phases.[29] Beyond 800 °C, the TGA curve reaches a stable plateau, displaying no additional mass loss. This thermal stability region confirms the selection of 800 °C as the final calcination temperature, ensuring full conversion to the layered oxide structure without further decomposition. Overall, the TGA profile supports the chosen thermal treatment route and confirms the precursor's complete transformation into a stable oxide phase at elevated temperatures.

The impact of different calcination temperatures on the crystallite size and phase purity of the synthesized NCM523 cathode materials is analyzed using XRD diffraction patterns and is shown in Fig. 4. The intensity ratios of the diffraction patterns of 003/104 planes and the degree of the peak splitting of 006/102 and 108/110 are a good indication of layered structure materials.[27,30] The NCM-800 diffraction peaks display the best layered structure with no discernible impurity reflections, and the creation of a typical layered structure is indicated by the obvious full splitting of the pair reflections of (006)/(102) and (108)/(110) (Fig. 4b). Since this displacement (Ni^{2+} at the 3a site and Li^{+} at the 3b site in the space group of layered $R\bar{3}m$) weakens the intensity of the (003) line without changing the intensity of the (104) peaks, the integrated intensity ratio of the (003) and (104) peaks is often employed to define the Li^{+}/Ni^{2+} cation mixing.[31] When the ratio is higher (>1.2), the degree of cation mixing is lower. We can find out that NCM-800 has a higher concentration value of 1.42 compared to the NCM-700 cathode

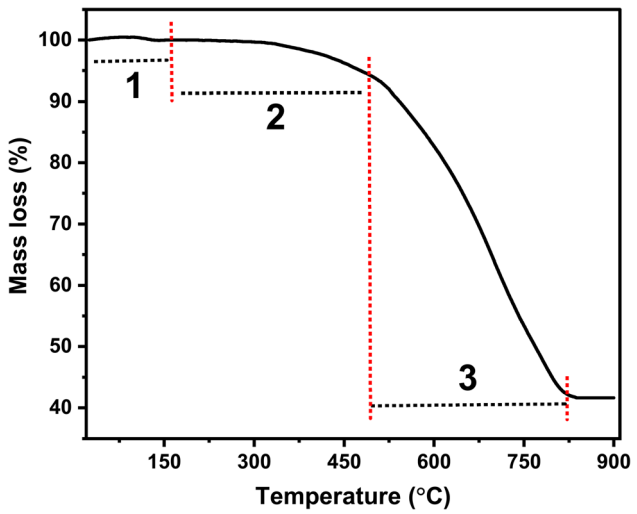

Fig. 3 TGA thermographs of the NCM523 precursor.

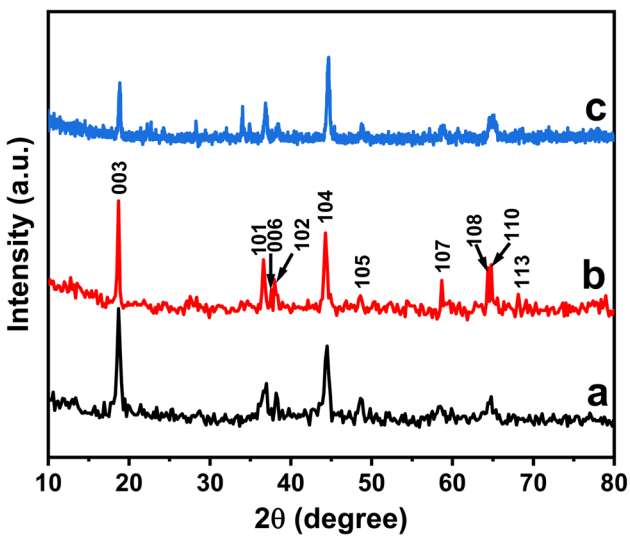

Fig. 4 XRD diffraction patterns of NCM523 cathode materials calcined at (a) 700 °C, (b) 800 °C, and (c) 900 °C.

materials (1.29) (Fig. 4a). At high calcination temperature (Fig. 4c), the intensity of the diffraction peak of the (003) plane significantly reduces to a minimum value compared to NCM-700 and NCM-800 cathode materials. The intensity ratio decreases to 0.76 because excessive calcination temperature causes structural degradation and increases cation mixing in NCM523 cathode materials. Compared to NCM-700, which shows broader XRD peaks indicative of poor crystallinity and possible structural defects, NCM-800 demonstrates sharper peaks, suggesting improved phase purity and reduced cation mixing. The crystallite size of the NCM523 samples varied noticeably with calcination temperature. At 700 °C, the crystallite size was 31 nm, demonstrating the primary growth of the layered structure. Increasing the temperature to 800 °C enhanced crystal growth, creating the largest crystallite size of 37 nm, which reflects improved crystallinity. However, further heating to 900 °C reduced the crystallite size to 26 nm, signifying structural instability and the onset of thermal degradation at excessively high temperatures.[32]

The Rietveld refinement of the NCM523 cathode materials calcined at 800 °C is shown in Fig. 5, and the values of lattice parameters for XRD patterns are calculated and summarized in Table 2. The analysis reveals well-defined lattice parameters of $a = 2.8755$ Å and $c = 14.1806$ Å, giving a c/a ratio of 4.9315, which is characteristic of a well-ordered $R\bar{3}m$ layered structure. A higher c/a ratio usually indicates better separation between the lithium and transition-metal layers and agrees with lower Li/Ni interlayer mixing.[33] This is consistent with the refined cation occupancy, which displays only 0.022 Ni present on the Li (3a) site, corresponding to a Li/Ni mixing level of around 2.2%. Such a low mixing percentage enables the 800 °C sample to maintain strong structural ordering, negligible cation disorder, and even layer stacking properties that typically boost lithium-ion diffusion and electrochemical performance.

Comparative FTIR spectra of the 700, 800, and 900 °C calcined samples display a significant influence of temperature on their purity and are shown in Fig. 6. NCM7 exhibits strong O–H stretching (at approximately 3400 cm^{-1}) and bending (at approximately 1620 cm^{-1}) bands, along with pronounced C–O vibrations, indicating incomplete decomposition of hydroxyl and organic species. At 800 °C, these peaks are significantly reduced, and the M–O stretching region of 520–650 cm^{-1} becomes sharper and more powerful, demonstrating enhanced crystallization and development of the layered NCM523 structure. Although the 900 °C precursor shows minimal organic signals, the M–O bands become broadened, signifying lattice distortion/defect generation at excessively high temperatures. These verdicts approve that 800 °C is the most favorable calcination temperature, providing the best balance between organic removal and structural ordering (Table 3).

The elemental composition and the variation of the oxidation state of each transition metal ion in the NCM523 cathode materials are detected using XPS spectra and are illustrated in Fig. 7. The survey spectra (Fig. 7a) of each cathode material show the spectra of Li 1s, C 1s, O 1s, Mn 2p, Co 2p, and Ni 2p without any impurities. The O 1s spectra of the NCM523 cathode materials are deconvoluted into three peaks that reflect distinct oxygen atmospheres within the material (Fig. 7b). The low binding energy peak at 529.2 eV resembles O^{2-} ions bonded to transition metals, representing stable lattice oxygen in the layered structure. The high binding energy peak at 531.4 eV

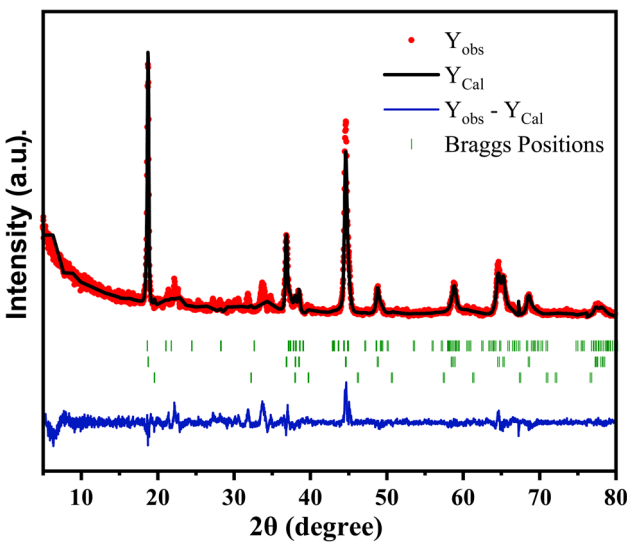

Fig. 5 Rietveld refinement results of NCM523 cathode materials calcined at 800 °C.

Table 2 Lattice parameter of the NCM8 sample

	Lattice parameters				
Sample	a (Å)	c (Å)	c/a	$I(003)/I(104)$	Li^+/Ni^{2+} mixing (%)
NCM8	2.8755	14.1806	4.9315	1.42	2.2

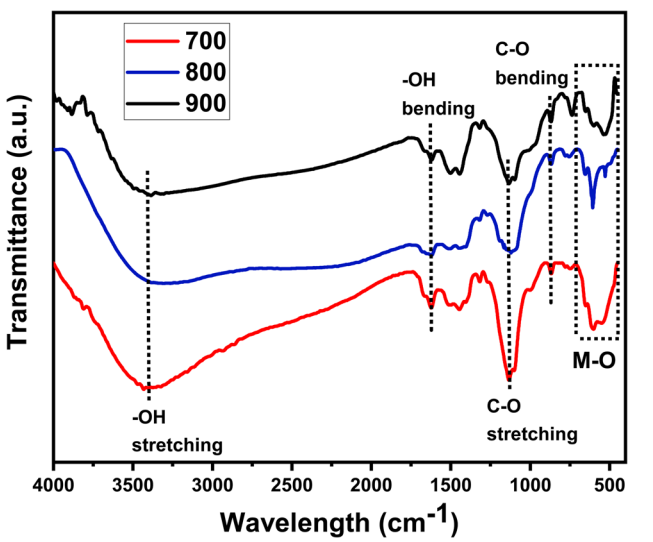

Fig. 6 FTIR spectra of NCM52 cathode materials at different calcination temperatures 700 °C (red line), 800 °C (blue line), and 900 °C (black line).

Table 3 Effect of calcination temperature on NCM523 cathode materials

Calcination temperature	O–H vibrations (3400 and 1620 cm^{-1})	C–O vibrations (1130 and 865 cm^{-1})	M–O bands (520–650 cm^{-1})	Interpretation
700 °C	Strong	Strong	Weak/broad	Incomplete decomposition, low structural order
800 °C	Reduced	Suppressed	Strong/sharp	Optimal layered oxide formation
900 °C	Minimal	Very weak	Broadened	Over calcination, lattice distortion

originates from surface species of $–CO_3$, adsorbed H_2O, and –OH groups. The intermediate peak (530.35 eV) from oxygen is involved in defect-rich regions, including vacancy-related O^{2-} or partially hydroxylated sites.[34] The spectrum also highlights that NCM-800 has the highest $O_{lattice}/O_{surface}$ ratio of 0.26, suggesting minimal oxygen vacancies and a well-developed metal–oxygen framework. In contrast, the NCM7 sample displays a much lower ratio (0.13), reflecting partial oxidation and the existence of surface-bound hydroxyls and carbonates due to insufficient thermal decomposition. The 900 °C sample also demonstrates a reduced ratio (0.11), which is attributed to excessive oxygen loss and defect generation at high temperature. The Li 1s spectrum of NCM-800 presents a sharp and well-defined peak at a binding energy of 58.5 eV, confirming effective lithium incorporation, unlike NCM-700, which has a weaker Li signal, or NCM-900, which shows signs of lithium loss[22] (Fig. 7c). The XPS spectra of Co 2p (Fig. 7d) consist of two main points of Co $2p_{3/2}$ (~780 eV) and Co $2p_{1/2}$ (~795 eV), along with corresponding satellite peaks at higher binding energies.[22] The 800 °C sample displays a Co^{2+}/Co^{3+} ratio of 0.24, indicating a dominant presence of Co^{3+}, which is characteristic of a well-formed layered structure with steady transition metal oxidation states. In comparison, the 700 °C sample shows a higher ratio (0.37), suggesting incomplete oxidation and a higher fraction of Co^{2+} associated with residual defects and hydroxyl groups. The 900 °C sample also presents an elevated ratio (0.31), which is typically associated with thermal over-reduction and increased surface defect formation. The peak position of Ni 2p in Fig. 7e of all three cathode materials shows doublet characteristic lines with the binding energy standards positioned at 854.6 eV and 873.5 eV, assignable to Ni $2p_{3/2}$ and Ni $2p_{1/2}$, respectively. The variation in binding energy between Ni $2p_{3/2}$ and Ni $2p_{1/2}$ of~18.9 is in good agreement with the standard references of Ni^{2+} cations.[35] The intensity of Ni $2p_{3/2}$ and Ni $2p_{1/2}$ lines was relatively high for NCM-800 cathode materials compared to the other two cathode materials, while it was minimal for the NCM-900 sample. Less noticeable peaks in the NCM-900 cathode material are seen at 856.0 and 874.5 eV, suggesting the existence of trace amounts of Ni^{3+} cations. A satellite peak around 861.9 eV was observed between the Ni $2p_{3/2}$ and Ni $2p_{1/2}$ regions, caused by the splitting of energy levels in nickel oxides. This splitting occurs due to the interaction of core electrons with the surrounding electron cloud in the nickel oxide structure, leading to a shift in binding energy.[33] The 800 °C sample displays a Ni^{2+}/Ni^{3+} ratio of 0.23, indicating efficient oxidation of Ni^{2+} to Ni^{3+} and a well-stabilized layered structure with limited cation disorder. In contrast, the 700 °C sample shows a noticeably lower ratio of 0.15, suggesting incomplete oxidation. The 900 °C sample, however, shows a markedly increased ratio of 0.89, which points toward thermal over-reduction and oxygen deficiency at elevated temperatures. Such a high Ni^{2+} content typically leads to increased Li^+/Ni^{2+} mixing and structural degradation. The Mn 2p spectrum of NCM-800 reflects the electron binding energy at 642.5 eV and 638.8 eV for Mn $2p_{3/2}$, which indicates the existence of both Mn^{2+} and Mn^{4+} ions.[33,36] The presence of both Mn^{2+} and Mn^{4+} ions contributes to phase stability, while NCM-700 exhibits some Mn^{4+}, which can lead to structural degradation. The 800 °C sample exhibits a Mn^{2+}/Mn^{4+} ratio of 0.52, representing a favorable distribution dominated by the electrochemically active Mn^{4+} state, which supports structural stability and suppresses Jahn–Teller distortions. At 700 °C, the ratio drops to 0.17, indicative of incomplete oxidation and a higher proportion of Mn^{2+} caused by insufficient thermal energy. Meanwhile, the 900 °C sample shows a ratio of 0.39, reflecting partial over-reduction and oxygen loss at excessively high temperatures (Table 4).

The particle morphology, size distribution, and structural integrity of the surfaces of NCM523 cathode materials calcined at different temperatures of 700 °C, 800 °C, and 900 °C were examined using FE-SEM and are shown in Fig. 8. The NCM523 cathode materials calcined at 700 °C are composed of small, loosely packed nanoparticles, and then these primary nanoparticles aggregate to form secondary particles with significant porosity, incomplete crystallization, and an irregular shape (Fig. 8a and b). At 800 °C, the NCM523 particles exhibit more uniform spherical secondary particles composed of tightly packed primary nanoparticles, with smooth surfaces and minimal cracks, indicating optimal crystallinity and agglomeration for balanced electrochemical performance. In contrast to NCM-800, excessive sintering at 900 °C results in larger, fused particles with microcracks and inhomogeneous grain growth, which degrade cycling stability and may exacerbate mechanical stress during charge/discharge (Fig. 8e and f). At 900 °C, particle size distributions become much wider, but at 800 °C, they maintain a small, Gaussian-like distribution perfect for long-term use and high tap density. These results are consistent with previous research, indicating that 800 °C is the ideal

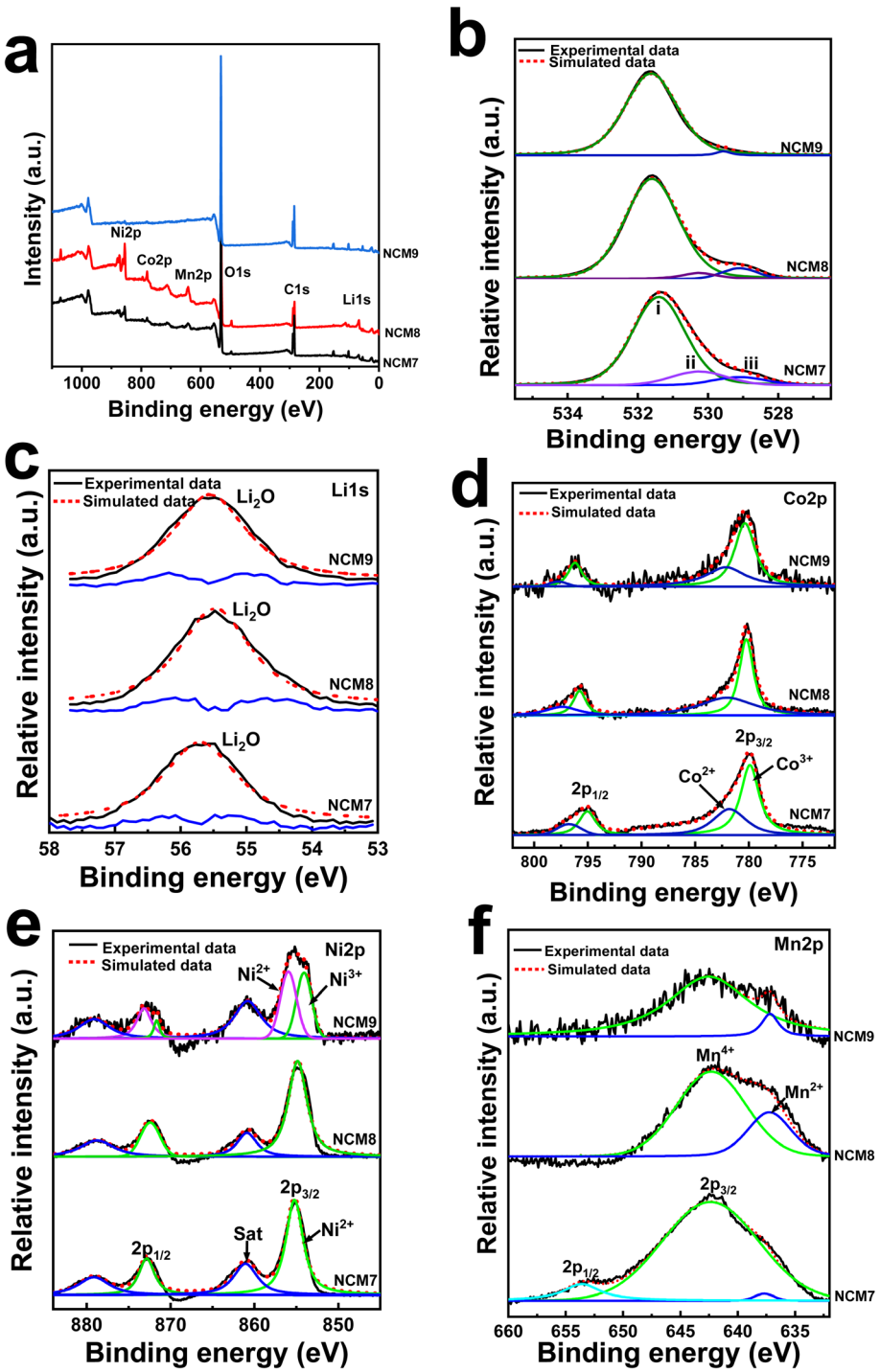

Fig. 7 X-ray photoelectron spectroscopy of (a) the survey spectrum and deconvoluted core line spectra of (b) O 1s, (c) Li 1s, (d) Co 2p, (e) Ni 2p, and (f) Mn 2p of NCM523 cathode materials, where NCM7, NCM8, and NCM9 indicate the calcined temperatures of 700 °C, 800 °C, and 900 °C, respectively.

Table 4 Summary of compositional and $O_{lattice}/O_{surface}$ ratios obtained from XPS analysis

Sample	Ni^{2+}/Ni^{3+}	Co^{2+}/Co^{3+}	Mn^{2+}/Mn^{4+}	$O_{lattice}/O_{surface}$
700 °C	0.15	0.37	0.17	0.13
800 °C	0.23	0.24	0.52	0.26
900 °C	0.89	0.31	0.39	0.11

calcination temperature for NCM523, striking a balance between particle uniformity, structural integrity, and electrochemical efficiency.[37]

The EDS analysis of NCM523 cathode materials calcined at 700 °C, 800 °C, and 900 °C provides crucial insights into elemental composition and distribution. The spectrum of the

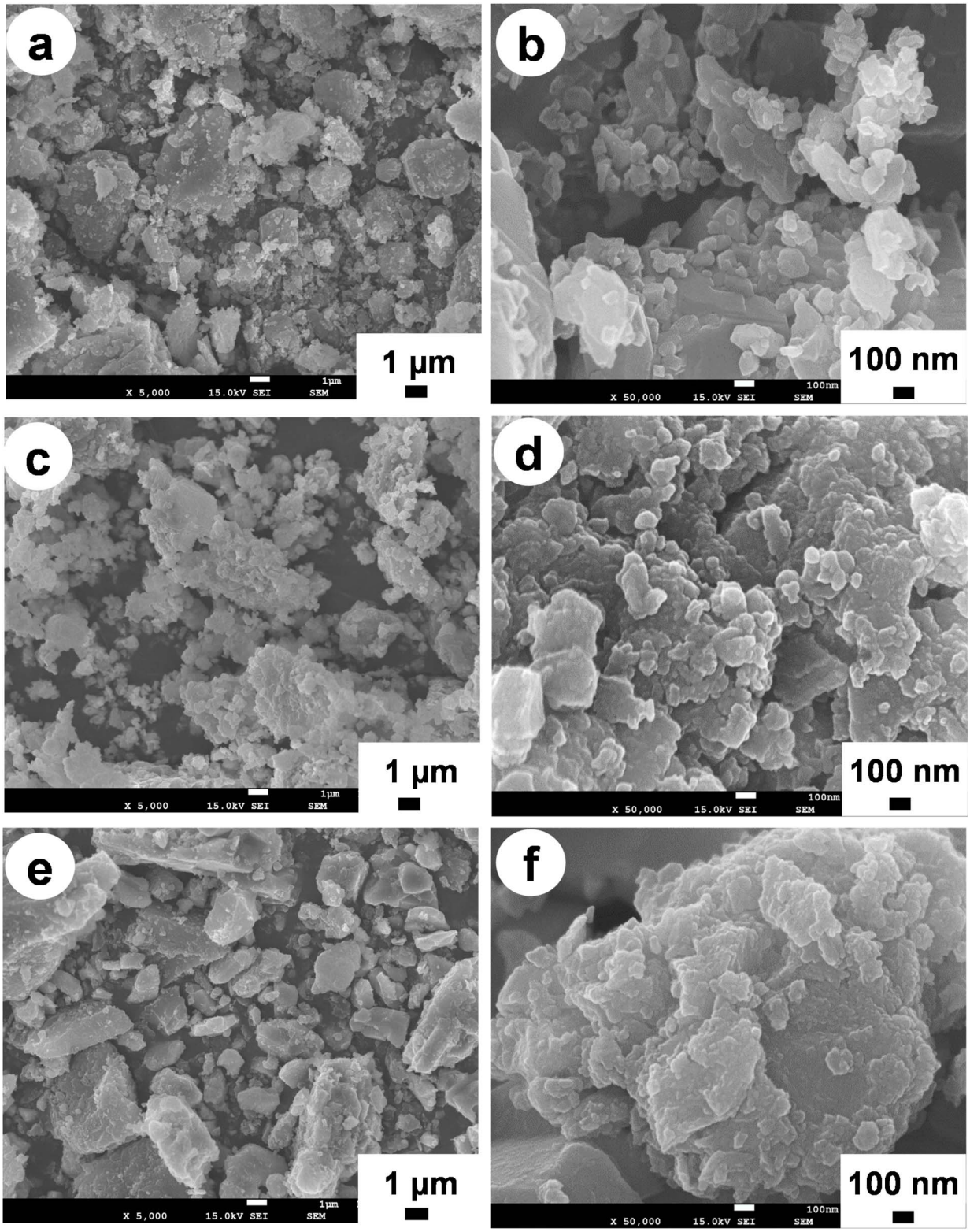

Fig. 8 FE-SEM images of NCM523 cathode materials at different magnification values (5k and 50k) calcined at (a and b) 700 °C, (c and d) 800 °C, and (e and f) 900 °C respectively.

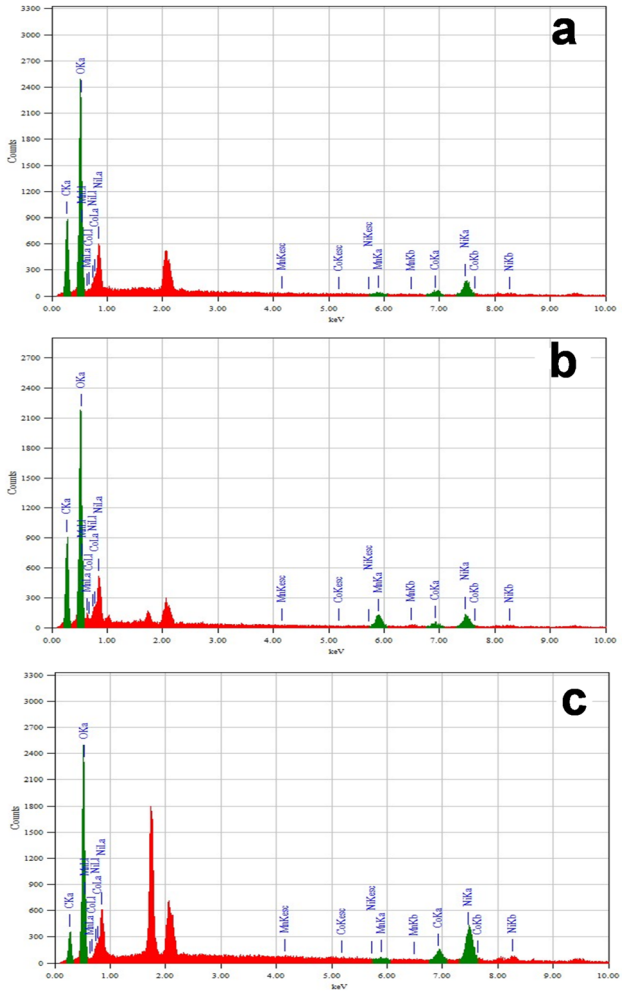

Fig. 9 EDS spectra of NCM523 cathode materials calcined at (a) 700 °C, (b) 800 °C, and (c) 900 °C.

700 °C sample (Fig. 9a) confirms the presence of Ni, Co, Mn, and O, but with signs of inhomogeneous distribution and possible residual Li_2CO_3 or LiOH, indicating incomplete crystallization. This cathode materials also exhibit deviation from the 5 : 2 : 3 stoichiometry (Ni ≈ 48.2%, Co ≈ 18.5%, and Mn ≈ 33.3%) with Mn surface segregation and residual Li_2CO_3 (C ≈ 5.2% and O ≈ 57%), indicating incomplete calcination, leading to poor cation diffusion. This suggests that the material may have phase impurities and an imbalanced Ni : Co : Mn ratio, which could negatively impact electrochemical performance. In contrast, the 800 °C sample (Fig. 9b) exhibits a highly uniform element distribution with near-ideal ratios (Ni ≈ 49.8%, Co ≈ 20.1%, and Mn ≈ 30.1%) with homogeneous cation distribution and minimal carbon (C ≈ 0.8%), ensuring structural integrity and the best balance of elements. However, the 900 °C sample (Fig. 9c) shows Ni depletion (≈44.7%) and Mn enrichment (≈33.5%) due to thermal-driven cation migration, resulting in Mn-rich grain boundaries and trace Ni reduction (≈5.1%) in the final composition, promoting Mn^{3+} Jahn–Teller distortion and oxygen loss. This may lead to structural degradation, elemental segregation, and cation migration, potentially reducing the cathode's long-term stability. Overall, the NCM-800 sample demonstrates the most favorable elemental distribution with minimal defects for high-performance NCM523 cathode materials.[37]

The TEM micrographs of the NCM523 sample calcined at 800 °C (Fig. 10) reveal well-developed primary particles and a highly crystalline layered structure. The low-magnification image (Fig. 10a) shows that the secondary particles exhibit an aggregated morphology with particle clusters in the sub-micron to micron range, which is characteristic of well-sintered layered oxide cathodes. The intermediate magnification TEM image (Fig. 10b) displays loosely packed primary nanoparticles with sizes typically below 200 nm. High-resolution TEM (Fig. 10c) confirms the formation of a well-ordered layered structure, as demonstrated by clear lattice fringes corresponding to the (003) plane with an interplanar spacing of d_{003} = 0.47 nm, which agrees well with the characteristic spacing of the trigonal $R\bar{3}m$ NCM523 cathode materials.[22] The sharp and continuous lattice fringes also indicate low structural defects and high crystallinity, further supporting that calcination at 800 °C provides optimal ordering and phase purity for NCM523.

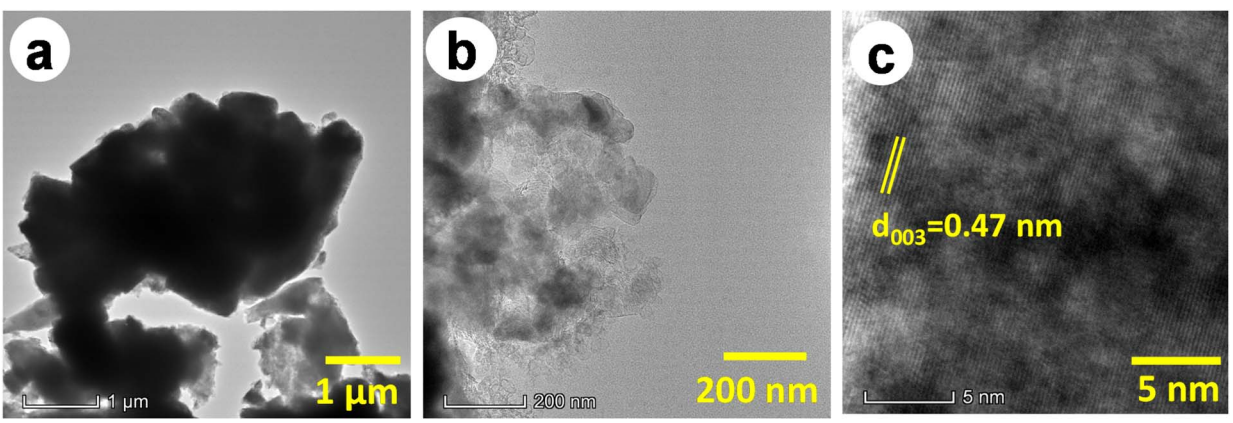

Fig. 10 TEM images at (a) low magnification and (b) high magnification and (c) HRTEM images of the NCM523 cathode material calcined at 800 °C.

Conclusion

In this investigation, particular emphasis is placed on developing a low-cost, environmentally friendly, thermally stable, and high-purity $LiNi_{0.5}Co_{0.2}Mn_{0.3}O_2$ (NCM523) cathode material. This work systematically demonstrates that both the solvent composition during precursor synthesis and the calcination temperature play critical roles in defining the final quality of NCM523 cathode materials. Among the evaluated solvent systems, the combination of EG, water, and EA proved superior due to its durable metal chelating capability, improved hydrolysis control, and ability to control nucleation kinetics. This synergy produced a highly uniform precursor that exhibited excellent crystallinity, well-resolved layered structural features, and the highest (003)/(104) intensity ratio (1.42) among all NCM523 cathode materials. FTIR investigation further established that this solvent system minimizes residual organic species and promotes the development of a stable M–O lattice network. Upon calcination, the 800 °C sample confirmed the optimal balance of crystallite growth, cation ordering, and oxygen stability, as demonstrated by its favorable Ni^{2+}/Ni^{3+}, Co^{2+}/Co^{3+}, and Mn^{2+}/Mn^{4+} ratios. The $O_{lattice}/O_{surface}$ value ratio reaches 0.26, significantly higher than at 700 °C (0.13) and 900 °C (0.11), confirming improved lattice oxygen stability and fewer surface defects. In contrast, lower temperatures led to incomplete oxidation and structural immaturity, while higher temperatures caused oxygen loss and defect generation. Therefore, the integrated approach of three solvent-assisted precursor synthesis followed by calcination at 800 °C yields the most phase-pure, structurally ordered, and chemically stable NCM523 material. These findings provide a comprehensive pathway for optimizing synthesis parameters to achieve high-performance layered cathode materials suitable for demanding lithium-ion battery technologies.

Author contributions

S. R.: data curation, formal analysis, investigation, validation, and writing – original draft. A. R.: formal analysis, investigation, methodology, visualization, validation, and writing – review and editing. R. H.: visualization. M. S.: investigation and validation. A. N. A.: formal analysis. M. S. Q.: formal analysis. C. K. R.: formal analysis. M. H.: writing – review and editing. M. S. J.: conceptualization, funding acquisition, project administration, validation, supervision, and writing – review and editing.

Conflicts of interest

The authors declare that they have no conflict of interest.

Data availability

The data underlying this article were produced during the course of the study and did not rely on external datasets, code, or specialized software.

Acknowledgements

This research was conducted as part of the R&D project (FY 2025–2028) of IERD, BCSIR, called "Synthesis and optimization of $LiNi_{1-x-y}Co_xMn_yO_2$ for use as cathode materials in advanced energy storage devices." We especially thank Shahran Ahmed Joy and Nadim Munna, scientific officer, Institute of Mining, Mineralogy and Metallurgy (IMMM), BCSIR, Joypurhat, for their support with Rietveld Refinement and TGA analysis.

References

1 H. Li, Y. Ren, P. Yang, Z. Jian, W. Wang, Y. Xing and S. Zhang, *Electrochim. Acta*, 2019, **297**, 406–416.
2 D. Ma, Y. Li, P. Zhang, A. J. Cooper, A. M. Abdelkader, X. Ren and L. Deng, *J. Power Sources*, 2016, **311**, 35–41.
3 H. Ding, X. Wang, J. Wang, H. Zhang, G. Liu, W. Yu, X. Dong and J. Wang, *J. Power Sources*, 2023, **553**, 232307.
4 B. Qiu, C. Yin, Y. Xia and Z. Liu, *ACS Appl. Mater. Interfaces*, 2017, **9**, 3661–3666.
5 Z. Cui, F. Zou, H. Celio and A. Manthiram, *Adv. Funct. Mater.*, 2022, **32**(36), 2203779.
6 B. Wu, H. Xu, D. Mu, L. Shi, B. Jiang, L. Gai, L. Wang, Q. Liu, L. Ben and F. Wu, *J. Power Sources*, 2016, **304**, 181–188.
7 P. S. Maram, G. C. C. Costa and A. Navrotsky, *Angew. Chem., Int. Ed.*, 2013, **52**, 12139–12142.
8 M. Y. Song and R. Lee, *J. Power Sources*, 2002, **111**, 97–103.
9 K. Vijaya Babu, L. Seeta Devi, V. Veeraiah and K. Anand, *J. Asian Ceram. Soc.*, 2016, **4**, 269–276.
10 X. Zhu, F. Meng, Q. Zhang, L. Xue, H. Zhu, S. Lan, Q. Liu, J. Zhao, Y. Zhuang, Q. Guo, B. Liu, L. Gu, X. Lu, Y. Ren and H. Xia, *Nat. Sustain.*, 2020, **4**, 392–401.
11 Y. Hong, C. Li, J. Ouyang, Q. Hu, X. Wang, Z. Tang and T. Liu, *Scr. Mater.*, 2024, **241**, 115878.
12 Y. Zhang, Q. Huo, P. Du, L. Wang, A. Zhang, Y. Song, Y. Lv and G. Li, *Synth. Met.*, 2012, **162**, 1315–1326.
13 K. Ben-Kamel, N. Amdouni, A. Mauger and C. M. Julien, *J. Alloys Compd.*, 2012, **528**, 91–98.
14 Y. Li, Q. Han, X. Ming, M. Ren, L. Li, W. Ye, X. Zhang, H. Xu and L. Li, *Ceram. Int.*, 2014, **40**, 14933–14938.
15 W. Liu, X. Li, Y. Hao, D. Xiong, H. Shan, J. Wang, W. Xiao, H. Yang, H. Yang, L. Kou, Z. Tian, L. Shao and C. Zhang, *Adv. Funct. Mater.*, 2021, **31**(13), 2008301.
16 C. Roitzheim, L.-Y. Kuo, Y. J. Sohn, M. Finsterbusch, S. Möller, D. Sebold, H. Valencia, M. Meledina, J. Mayer, U. Breuer, P. Kaghazchi, O. Guillon and D. Fattakhova-Rohlfing, *ACS Appl. Energy Mater.*, 2022, **5**, 524–538.
17 X. Dai, A. Zhou, J. Xu, B. Yang, L. Wang and J. Li, *J. Power Sources*, 2015, **298**, 114–122.
18 S. Shi, T. Wang, M. Cao, J. Wang, M. Zhao and G. Yang, *ACS Appl. Mater. Interfaces*, 2016, **8**, 11476–11487.
19 J. Zheng, W. Zhou, Y. Ma, H. Jin and L. Guo, *J. Alloys Compd.*, 2015, **635**, 207–212.
20 M. Jiang, Q. Zhang, X. Wu, Z. Chen, D. L. Danilov, R.-A. Eichel and P. H. L. Notten, *ACS Appl. Energy Mater.*, 2020, **3**, 6583–6590.

21 X. Jiang, Y. Sha, R. Cai and Z. Shao, *J. Mater. Chem. A*, 2015, **3**, 10536–10544.
22 J. Fang, H. An, F. Qin, H. Wang, C. Chen, X. Wang, Y. Li, B. Hong and J. Li, *ACS Appl. Mater. Interfaces*, 2020, **12**, 55926–55935.
23 X. Hou, Y. Huang, S. Ma, X. Zou, S. Hu and Y. Wu, *Mater. Res. Bull.*, 2015, **63**, 256–264.
24 Y. Liu, T. Moser, C. Andres, L. Gorjan, A. Remhof, F. Clemens, T. Graule, A. N. Tiwari and Y. E. Romanyuk, *J. Mater. Chem. A*, 2019, **7**, 3083–3089.
25 S. Dong, Y. Zhou, C. Hai, J. Zeng, Y. Sun, Y. Shen, X. Li, X. Ren, G. Qi and L. Ma, *Ionics*, 2019, **25**, 5655–5667.
26 W. Ahn, S. N. Lim, K.-N. Jung, S.-H. Yeon, K.-B. Kim, H. S. Song and K.-H. Shin, *J. Alloys Compd.*, 2014, **609**, 143–149.
27 Y. Sun, Y. Zhou, L. Zhang, Y. Shen and J. Zeng, *J. Alloys Compd.*, 2017, **723**, 1142–1149.
28 C. S. Yudha, S. U. Muzayanha, H. Widiyandari, F. Iskandar, W. Sutopo and A. Purwanto, *Energies*, 2019, **12**(10), 1886.
29 J. P. Yasnó, S. Conconi, A. Visintin and G. Suárez, *J. Anal. Sci. Technol.*, 2021, **12**, 15.
30 F. Wu, M. Wang, Y. Su, L. Bao and S. Chen, *J. Power Sources*, 2010, **195**, 2362–2367.
31 J. Zhu, J. Zheng, G. Cao, Y. Li, Y. Zhou, S. Deng and C. Hai, *J. Power Sources*, 2020, **464**, 228207.
32 J. Li, M. Zhang, D. Zhang, Y. Yan, Z. Li and Z. Nie, *Int. J. Electrochem. Sci.*, 2020, **15**, 1881–1892.
33 Y. Zhang, C. Cui, Y. He, J. Liu, Y. Song, Z. Song, H. Xu, S. Huang and Y. Bei, *Mater. Chem. Phys.*, 2021, **262**, 124269.
34 A. Sharma, R. Abdur, D. Kim, A. K. Tripathi, S. Singh, J. Lee and S. I. Yoo, *Curr. Appl. Phys.*, 2020, **20**, 1041–1048.
35 M. Cheng, H. Fan, Y. Song, Y. Cui and R. Wang, *Dalton Trans.*, 2017, **46**, 9201–9209.
36 S. Dong, Y. Zhou, C. Hai, J. Zeng, Y. Sun, Y. Shen, X. Li, X. Ren, G. Qi and L. Ma, *Ionics*, 2019, **25**, 5655–5667.
37 W. Ahn, S. N. Lim, K.-N. Jung, S.-H. Yeon, K.-B. Kim, H. S. Song and K.-H. Shin, *J. Alloys Compd.*, 2014, **609**, 143–149.